Large-Scale User Facility Imaging and Scattering Techniques to Facilitate Basic Medical Research

Stephen D. Miller[1], Jean-Christophe Bilheux[1], Shaun S. Gleason[2],
Trent L. Nichols[2], Philip R. Bingham[2] and Mark L. Green[3]
[1]Neutron Scattering Science Division, Oak Ridge National Laboratory
[2]Measurement Science & Systems Engineering Division
Oak Ridge National Laboratory
[3]Tech-X Corporation
USA

1. Introduction

Conceptually, modern medical imaging can be traced back to the late 1960's and into the early 1970's with the advent of computed tomography[1]. This pioneering work was done by 1979 Nobel Prize winners Godfrey Hounsfield and Allan McLeod Cormack which evolved into the first prototype Computed Tomography (CT) scanner in 1971 and became commercially available in 1972. Unique to the CT scanner was the ability to utilize X-ray projections taken at regular angular increments from which reconstructed three-dimensional (3D) images could be produced. It is interesting to note that the mathematics to realize tomographic images were developed in 1917 by the Austrian mathematician Johann Radon who produced the mathematical relationships to derive 3D images from projections – known today as the Radon Transform[2]. The confluence of newly advancing technologies, particularly in the areas of detectors, X-ray tubes, and computers combined with the earlier derived mathematical concepts ushered in a new era in diagnostic medicine via medical imaging (Beckmann, 2006).

Occurring separately but at a similar time as the development of the CT scanner were efforts at the national level within the United States to produce user facilities to support scientific discovery based upon experimentation. Basic Energy Sciences[3] within the United States Department of Energy[4] currently supports 9 major user facilities along with 5 nanoscale science research centers dedicated to measurement sciences and experimental techniques supporting a very broad range of scientific disciplines. Tracing back the active user facilities,

---

[1] Computed Tomography and History: http://en.wikipedia.org/wiki/Computed_tomography
[2] Radon Transform: http://en.wikipedia.org/wiki/Radon_Transform
[3] US DOE Basic Energy Sciences User Facilities:
http://science.energy.gov/user-facilities/basic-energy-sciences/
[4] US DOE: http://science.energy.gov/

the Stanford Synchrotron Radiation Lightsource[5] (SSRL) a SLAC National Accelerator Laboratory was built in 1974 and it was realized that its intense x-ray beam could be used to study protein molecular structure. The National Synchrotron Light Source[6] (NSLS) at Brookhaven National Laboratory was commissioned in 1982 and currently has 60 x-ray beamlines optimized for a number of different measurement techniques including imaging and tomography. The next generation NSLS-II facility is now under construction. The Advanced Light Source[7] (ALS) commissioned in 1993 has one of the world's brightest sources of coherent long wavelength x-rays suitable for probing biological samples in 3D. The Advanced Photon Source[8] at Argonne National Laboratory also has a number of x-ray beamlines dedicated to imaging and tomography suitable for biological and medical imaging research. The Spallation Neutron Source[9] (SNS) at Oak Ridge National Laboratory (ORNL) also has a number of beamlines suitable for studying the structure and dynamics of proteins and other biological systems. A neutron imaging and tomography beamline is currently being planned for SNS. Similarly, the High Flux Isotope Reactor[10] (HFIR) also at ORNL has beamlines suitable for examining biological matter and has an operational imaging beamline. In addition, the production of medical isotopes is another important HFIR function.

These user facilities have been intended to facilitate basic and applied research and were not explicitly designed with the intention to scan patients the same way commercial medical imaging scanners do. Oftentimes the instrument beam power is significantly more powerful than that produced by medical scanners. Thus the ionizing radiation effects of these beams must be considered when contemplating how these facilities can contribute to medical research. Suitable research areas involving user facilities include the study of proteins, human and animal tissue sample scanning, and in some cases, the study of non-human vertebrate animals such as various rodent species. The process for scanning biological and animal specimens must be approved by the facility biosafety review board.

However there is still a significant amount of bio and medical related research being performed at these national laboratory user facilities and below is a sampling of some of the published research which utilized imaging and scattering resources available via the above mentioned national laboratories:

- At NSLS: The study of thrombosis in rats utilizing Micro- and Nano-CT (Stolz et al., 2011), density quantification of Vasa Vasorum in tomographic coronary angiograms (Moritz et al., 2010), Micro-CT imaging of the human lung acinus (Litzlbauer et al., 2010), rat bone imaging (Rao et al., 2009), bone density using iliac crest biopsies (Jorgensen et al., 2008).
- At APS: sparse data reconstruction of biomedical samples using micro-tomography (Xiao et al., 2010), trabecular bone sample imaging (Xiao et al., 2008), high-energy x-ray scattering of a cortical bone specimen (Stock et al., 2008), visualization of trace metals in biological tissue (D de Jonge & Vogt, 2010).

---

[5] SSRL: http://www-ssrl.slac.stanford.edu/

[6] NSLS: http://www.nsls.bnl.gov/

[7] ALS: http://www-als.lbl.gov/

[8] APS: http://www.aps.anl.gov/

[9] SNS: http://neutrons.ornl.gov/facilities/SNS/

[10] HFIR: http://neutrons.ornl.gov/facilities/HFIR/

- At ALS: irradiation effects on human cortical bone fracture behavior (Barth et al., 2010), x-ray diffraction microscopy of whole biological cells (Nelson et al., 2010), and soft x-ray tomography to image antifungal drug molecules in action (Uchida et al., 2009).
- At SSRL: cell-cell and cell-matrix adhesion molecules (Choi & Weis, 2011), crystallographic analysis (Gupta & Kielkopf, 2011), X-ray absorption spectroscopy for DNA repair (Giri et al., 2011).
- At SNS & HFIR: protein-protein interactions in DNA replication and repair (Hinerman, 2008), lysosome diffusion dynamics of hydration water (Zhang et al., 2009), and enzymatic studies in aqueous ionic liquids (Baker & Heller, 2009).

Each of these facilities utilizes a similar process for how to get beam time at the instruments. There are periodic calls for proposals to which competing proposal teams will respond with descriptions of the experiments they seek to perform while also citing their experiment goals and objectives. Once the proposal call is closed, the proposals are reviewed by a committee comprised of technical experts from a variety of different research and academic institutions. The first pass is a feasibility review to determine if the proposed experiment can be done at the beamline for which time has been requested. This feasibility review will consider things such as the sample environment required, the nature of the material should it be hazardous in some way, and the experiment needs versus the resolution and capabilities of the instrument. The proposals that pass the feasibility review are then peer reviewed by an external scientific review committee which rates and rank the proposals. Subsequently, a beam time allocation committee will make determinations on the amount of time each experiment will then get according to the scientific review committee findings. The outcome will be a list of accepted and alternate proposals and the facility User Office will then initiate making contact with the corresponding experiment Principal Investigators informing them that their proposals have been accepted. As part of the scheduling process, the instrument team will interact with the approved experiment teams to determine experiment dates. As part of scheduling, a local contact will be assigned to each experiment team. This local contact is a valuable asset to the experiment team as this person will assist as necessary to help with making the experiment a success.

Each of these user facilities is a part of the national laboratory in which it resides. As such, there are a number of potential resources available to the research teams which may vary according to the capabilities, personnel, and support facilities available within a particular national laboratory. Across the national laboratory system, five Nanoscale Science Research Centers have been built, and one function of these centers is to help facilitate scientific research at the experimental user facilities. These centers include:

- Center for Nanophase Materials Sciences[11] (CNMS) at ORNL which provides clean rooms, wet and dry labs, sample fabrication, and analysis. CNMS is co-located with SNS to help provide unique capabilities for neutron scattering.
- Molecular Foundary at Lawerence[12] Berkeley National Laboratory which provides laboratories for material science, chemistry, biology, and molecular biology utilizing clean rooms, controlled environment rooms, DNA synthesizer and sequencer, NMR spectrometer, mass spectrometers, along with scanning tunnelling, transmission electron, fluorescence microscopes.

---

[11] CNMS: http://www.cnms.ornl.gov/
[12] Molecular Foundary: http://foundry.lbl.gov/

- Center for Integrated Nanotechnologies[13] (CINT) jointly administered by Los Alamos National Laboratory[14] (LANL) and Sandia National Laboratory[15] (SNL). CINT focus areas are nanophotonics and nanoelectronics, complex functional nonomaterials, nonomechanics, and the nonoscale/bio/microscale interfaces.
- Center for Functional Nanomaterials[16] (CFN) is located at Brookhaven National Laboratory[17] (BNL). CFN develops understandings of the chemical and physical nature of nanomaterials in order to make functional materials such as sensors, activators, and energy conversion devices.
- Center for Nanoscale Materials[18] (CNM) is located at Argonne National Laboratory[19] (ANL) and focuses on research pertaining to advanced magnetic materials, complex oxides, nanophotonics, and bio-inorganic hybrid materials.

In addition to these centers, the national laboratories have unique capabilities to interpret the data that is generated by these facilities. For example, the Imaging, Signals, and Machine Learning (ISML) group[20] within ORNL has expertise in imaging, image/data understanding, and machine learning methods to turn large experimental data sets into useful information for the scientist. A few of the relevant active research capabilities include high-resolution neutron image capture (new scintillators, coded apertures, etc.), tomographic reconstruction, and post reconstruction image analysis and data understanding. Application areas include biomedical imaging[21], telemedicine for retinal diagnostics, CAD for mammography, small animal high-resolution micro-tomographic medical imaging, image analysis for organ segmentation, neuron image analysis and phenotype screening. Such capabilities to analyze and interpret data are an important component of such user facilities to ensure that the ultimate goal of extraction of information from the collected data can be realized.

The remainder of this chapter will now examine the imaging and scattering capabilities of these instruments with special considerations for neutron imaging.

2. Imaging and scattering techniques

The measurement techniques at these user facilities vary more widely than those currently employed routinely within the field of medical imaging. In addition to traditional planar and tomographic imaging, additional scattering techniques such as spectroscopy, diffraction and small angle scattering are employed. In these cases, the scattered neutrons or x-rays are fit to physical models in order to determine structure or dynamics (Pynn, 1990). Structures can be at the atomic, molecular, or macro-molecular size scale depending upon the wavelength of the probing beam. An important distinction between x-ray and neutron scattering is that x-rays interact with the electron cloud while neutrons scatter off of the atomic nucleus. Thus in conceptual thinking, x-ray attenuation is approximately linear

---

[13] CINT: http://cint.lanl.gov/

[14] LANL: http://www.lanl.gov

[15] SANDIA: http://www.sandia.gov

[16] CFN: http://www.bnl.gov/cfn

[17] BNL: http://www.bnl.gov/

[18] CNM: http://nano.anl.gov/index.html

[19] ANL: http://www.anl.gov

[20] ISML: http://www.ornl.gov/sci/ees/mssed/isml/index.shtml

[21] ISML Biomedical Imaging: http://www.ornl.gov/sci/ees/mssed/isml/research-bio.shtml

according to the material density. However this is not the case with neutrons as the scattering cross section[22] is not linear with element density and neutrons scatter quite well off of hydrogen atoms where, in contrast, these atoms are difficult to image with x-rays, but aluminum and other metals are relatively transparent to neutrons. Thus these potentially complementary attenuation properties are useful to exploit for what they can provide.

2.1 Imaging

Contrasting imaging instruments and commercial medical imaging scanners reveals a drastically different scale required for hosting the devices. Typically the largest portion of the user facility is required to produce the interrogating beam. These beams have high power and can typically be shaped to produce a beam bandwidth of interest. Thus the instruments must be located at the facilities and people must come to them unlike the situation where many of the medical imaging modalities can be small enough to be mobile. Another important factor to consider is that imaging biological specimens, laboratory animals, and in rare cases, human tissue is the exceptions and not the rule for these facilities. To start with, one must make a convincing case via their proposal that it is worthwhile to scan the subject of interest. Then one must be prepared for additional scrutiny and review by the appropriate facility biological and bio-hazard review committees. Upon acceptance, one must then be prepared to follow proper specimen handling procedures. Note that science areas such as protein crystallography and soft matter are much more routine than described above. The instruments at the user facilities have powerful capabilities and one must carefully prepare in order to utilize them.

Despite these obstacles, there are active communities of researchers which utilize imaging instruments to help with their research. The context here for the definition of imaging refers to the various X-ray and neutron imaging instruments. Conceptually these instruments produce images in similar format as those produced by medical imaging scanners, however these instruments typically incorporate more flexibility for their capabilities and are less specialized and optimized as compared to the medical scanners. To illustrate imaging capabilities, some examples showing the differences in image contrast between neutron and x-ray imaging are shown in figures 1 through 3.

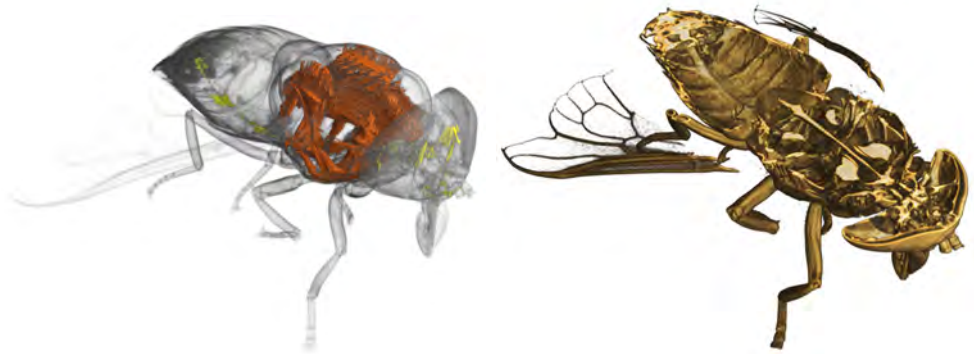[22] Neutron scattering cross sections: http://www.ncnr.nist.gov/resources/n-lengths/list.html

Fig. 1. Neutron tomography of a dried horsefly. Top right: outer surface, top left: upper portion sliced away, bottom right: mid-level slice, bottom left: contour of wing muscles. Note that the insect is approximately 1cm in length head to tail. Images courtesy of Dr. Eberhard Lehmann using the ICON beamline, SINQ, Paul Scherrer Institut, Switzerland[23].
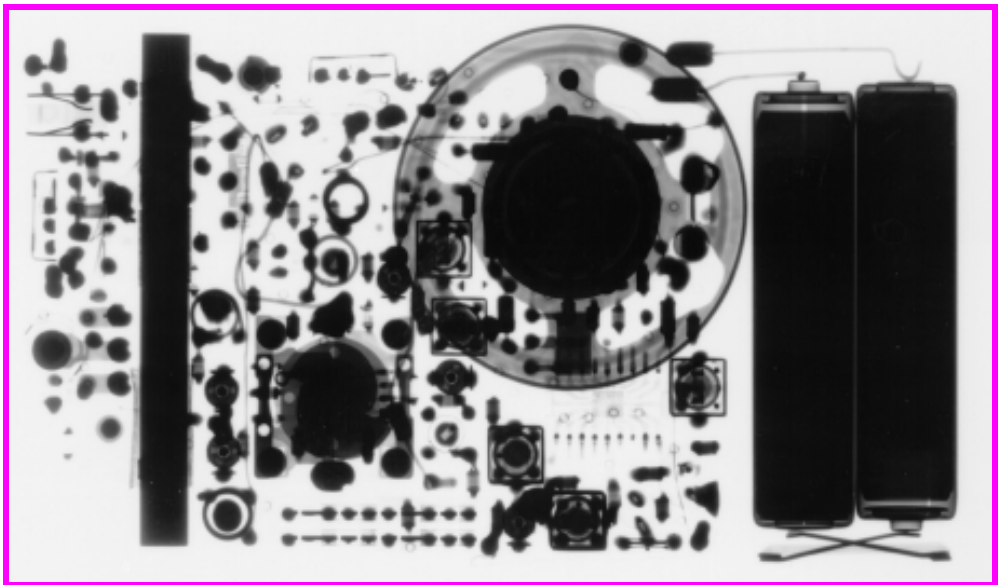
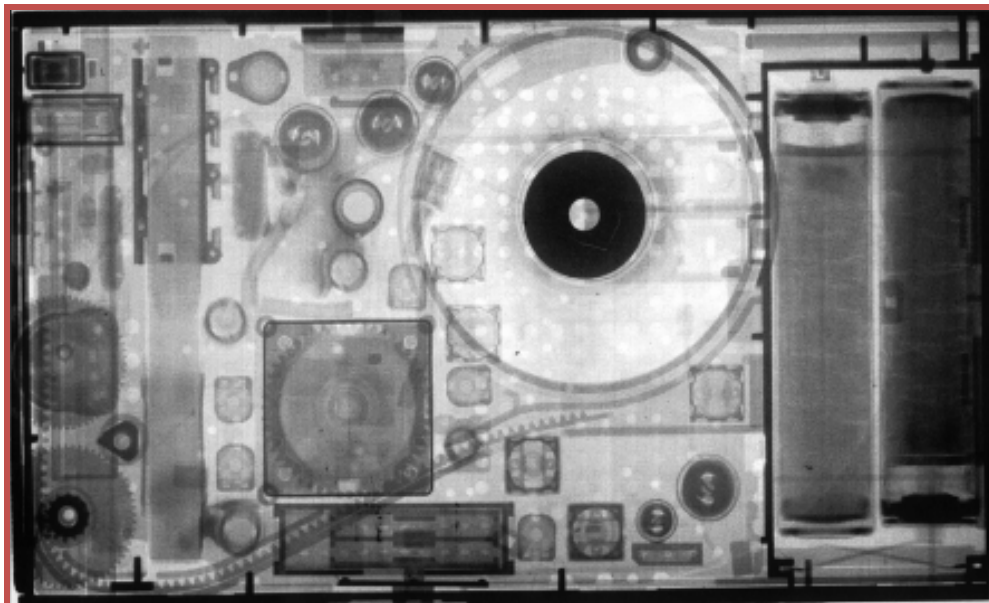[23] ICON Instrument: http://neutra.web.psi.ch/facility/icon_index.html

Fig. 2. X-ray (top) and neutron (bottom) images of a miniature transistor radio. Images courtesy of Dr. Eberhard Lehmann taken using the ICON beamline, SINQ, Paul Scherrer Institut, Switzerland.
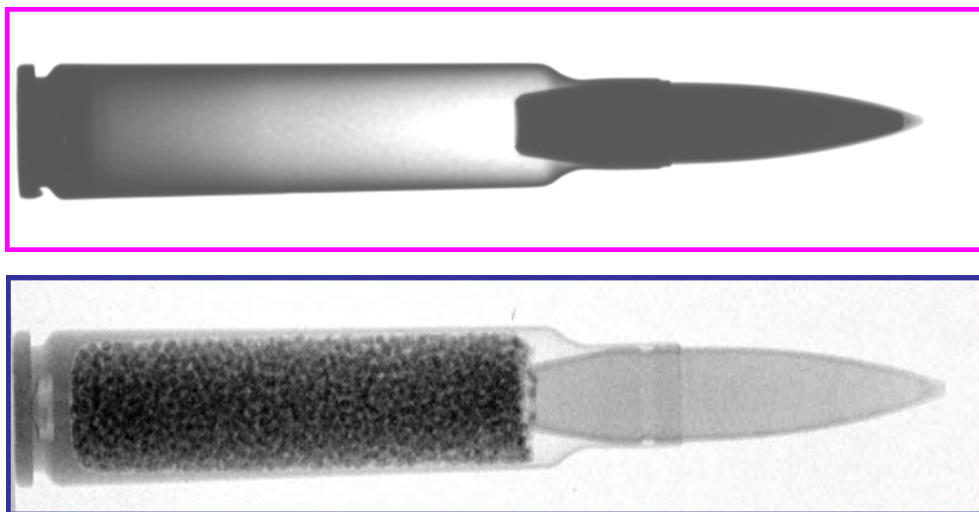

Fig. 3. X-ray (Top) and neutron (Bottom) image of a bullet. Note the difference in contrast where x-rays image illustrate metal density while neutrons are capable of imaging through metals to image materials containing hydrogen atoms. Images courtesy of Dr. Eberhard Lehmann taken using the ICON beamline, SINQ, Paul Scherrer Institut, Switzerland.

2.2 Scattering

From a medical imaging perspective, the usual case is to observe the attenuation pattern based upon the beam which transmits through the object being imaged. For tomography, a set of views are taken at angular increments around the object.

However a portion of the beam can scatter off of the object and can be detected outside the boundaries of the transmission image, and scattering techniques exist for both neutron and x-rays. For neutron scattering, a strong scattering object will scatter ~10% or less of the total transmission flux. The scattering angle can be vary across 4π Steradians (sr) depending upon a number of factors including beam properties such as wavelength and material properties such as structure. A conceptual illustration of transmission and small angle scattering is shown in figure 4. In contrast with transmission imaging, scattering detection systems may
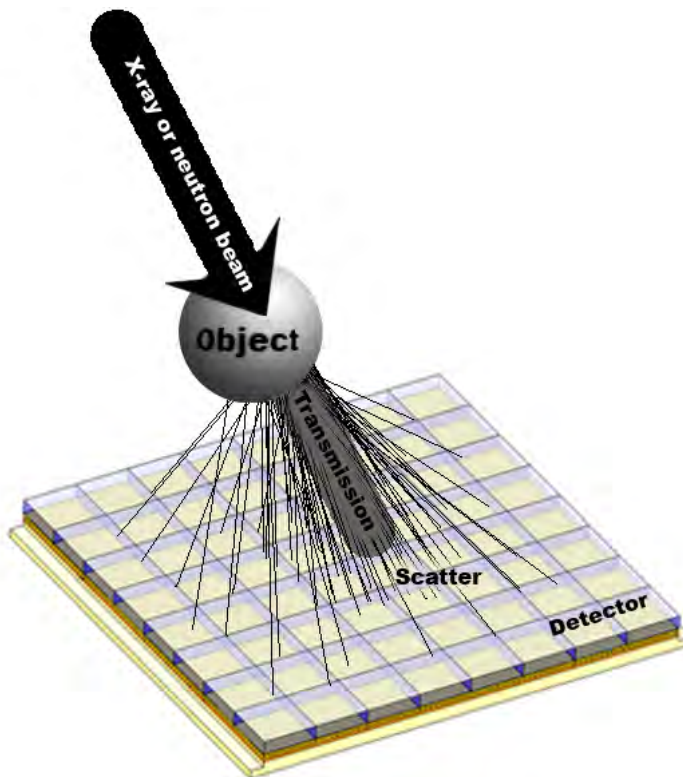
Fig. 4. Cartoon illustrating transmission and scatter detection locations for an object in an X-ray or neutron beam. Typically only one technique will be employed at a time but shown here together to illustrate differences between the detection techniques. The transmission image results from rays which strike the detector having passed directly through the object. The scatter pattern results from the rays being deflected at some angle here shown as small angle scattering though the scattering angles can be arbitrary in solid angle depending upon the sample and imaging beam characteristics.

utilize very small samples in comparison to the detector sizes. For example, a 1 cm³ size sample or smaller is typical while the detection system sizes may range to 10+ meters tall in order to obtain the desired solid angle detection range. Other scattering systems fix detectors about the sample covering as much of the 4π space as possible. The necessary distance between the sample and the detectors must be considered when spacing the detectors so as to take into consideration adequate resolution, and this distance may be several meters for some instruments.

There are a number of elastic scattering techniques including small angle scattering shown in figure 5, reflectometry, powder and single crystal diffraction. There also exist inelastic scattering techniques such as direct and indirect geometry spectrometry. Typically the scatter patterns are not as visually intuitive as the transmission images as one must deduce the structure via model fitting in the case for scattering science. As previously mentioned, a good primer for neutron scattering has been written by Pynn (Pynn, 1990). For examining the statistical nature of structure, scattering techniques can be used to measure a wide range of length scales ranging from atomic to molecular, to macromolecular and thus has its advantages over other measurement techniques.
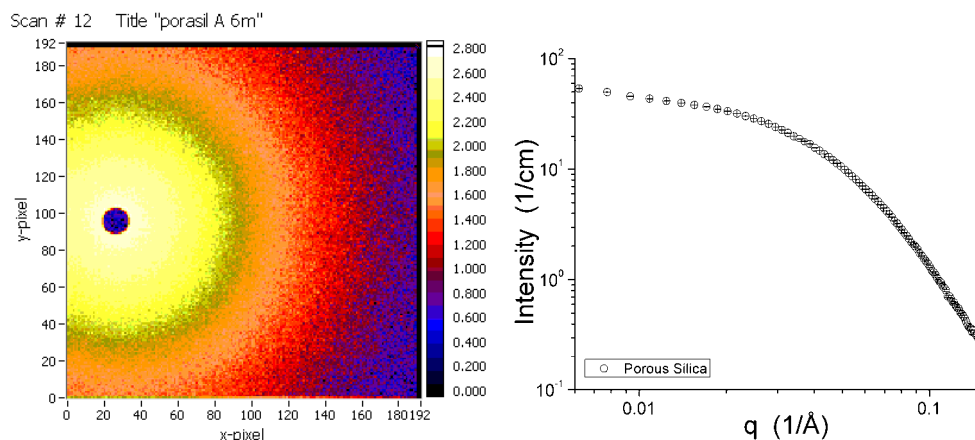

Fig. 5. Neutron scattering image of porous silica from a Small Angle Neutron Scattering instrument. Left: The raw detector data image – note that the center of scattering is offset to the left center of the image in this case to extend visibility of the data "tails" at the edge of the scattering pattern. Right: the corresponding reduced data illustrating intensity versus inverse Angstroms. Models can be fit to the reduced data to determine structure. Images courtesy of Dr. William T. Heller of the Spallation Neutron Source at Oak Ridge National Laboratory.

3. Neutron imaging beamline overview

The following section illustrates from acquisition to visualization working with neutron imaging data. The detection systems are explored as well as the processes for normalizing data and reconstructing images. A section discussing data management pertinent to the national laboratories is also included which illustrates some significant differences in data handling between the research and commercial medical imaging communities.

3.1 Data acquisition

Neutron radiography systems follow the same basic geometric design as x-ray system, so those familiar with resolution and magnification in x-ray systems will quickly feel comfortable working with neutrons. There are very few neutron imaging instruments, and they are built to accommodate a variety of types of materials research, so these instruments are designed to be flexible in their geometry in order to satisfy imaging requirements over a broad spectrum of applications from industrial to medical to archeological applications. This flexibility requires the user to have a basic understanding of neutron imaging instrument components and geometries to plan successful experiments. While the x-ray and neutron system geometries are similar, the commonly used designs are different due to differences in the available sources and detectors. Since x-ray and neutron imaging are so similar and x-ray is a well accepted and understood imaging modality, the following discussion of neutron radiography system will draw parallels and point out differences between the systems through the description of the sources, detectors, and geometric designs.

3.1.1 Neutron sources

Neutron sources for radiography are large user facilities that are either reactor sources producing a continuous beam of neutrons or spallation sources producing neutron pulses (Arai & Crawford, 2009). Since the neutrons from both types of source are initially higher in energy than would be useful for most scattering and imaging experiments, the neutrons are passed through a moderator that scatters the neutrons to lower their energy. As a result of creating a large initial source to emit as many neutrons as possible and use of a moderator, neutron sources are quite large with ports to instruments having sizes in the tens of centimeters. In contrast, x-ray sources with similar flux are available having spot sizes down to 5μm in diameter. The large source size for neutrons is a key issue when designing the imaging geometry as discussed later.

Pulsed sources for both x-rays and neutrons can be used like a flash bulb to stop motion of the object being imaged; however, the reason for building pulsed neutron sources such as the SNS is to provide energy resolution. The speed that a neutron travels is directly proportional to the energy of the neutron; therefore, a neutron pulse spreads out over distance traveled. By placing a detector with timing resolution a sufficient distance from the source, images can be obtained over a range of neutron energies (wavelengths). In medical imaging, we see dual energy x-ray systems used to enhance the contrast between materials in the body and also achieve some level of elemental analysis. This is possible because a material's x-ray attenuation coefficient is a function of the x-ray energy, and this function varies between materials. For example, a dual energy X-ray image can determine if a kidney stone is composed of uric acid or if it contains calcium. Another common use of dual energy x-ray is to calculate bone mineral density for diagnosis of osteoporosis or osteopenia. Finally, dual (or more) energy x-rays are commonly used to enhance images of lung parenchyma because the bones can be removed from the final image. In this same sense, imaging over a range of neutron energies can provide contrast for different materials and even identify materials based on the transmission spectrum. One area of interest for imaging at multiple wavelengths is with respect to crystal structures and may have applications in imaging of interfaces between tissue and prosthetic joint devices. The polycrystalline materials of these metal joints has a unique transmission spectrum with large swings in attenuation at particular energies known as Bragg edges.

Imaging on both sides of a Bragg edge will provide two very different contrast images to help identify the interface between tissue, bone, and prosthetic device.

3.1.2 Neutron imaging devices

Two types of direct digital imaging devices are employed at neutron imaging instruments: scintillator based and micro channel plate (MCP) based. MCP based detectors provide the higher resolution than scintillators for neutron radiography, but they are much more expensive and degrade with use.

Scintillator based imaging devices use a ^{6}Li based scintillator plate to convert neutrons to visible light which is imaged by a CCD or CMOS based camera as shown in figure 6. In these systems, a mirror is used to move the camera out of the direct neutron beam for protection of the electronics and to remove components that may become activated by the neutron beam and as a result produce noise in the images due to gamma ray emissions striking the CCD or CMOS electronics. The right side of this figure is a photograph of a scintillator based camera in use at HFIR.

The highest resolution of scintillator based neutron imagers is approximately 50μm and is a function of the scintillator, the lens, and the CCD or CMOS detector. Currently the resolution is limited by the scintillator resolution. ^{6}Li Scintillator screens are available in varying thicknesses. Thinner screens provide the highest resolution but interact with fewer neutrons which leads to longer exposure times.
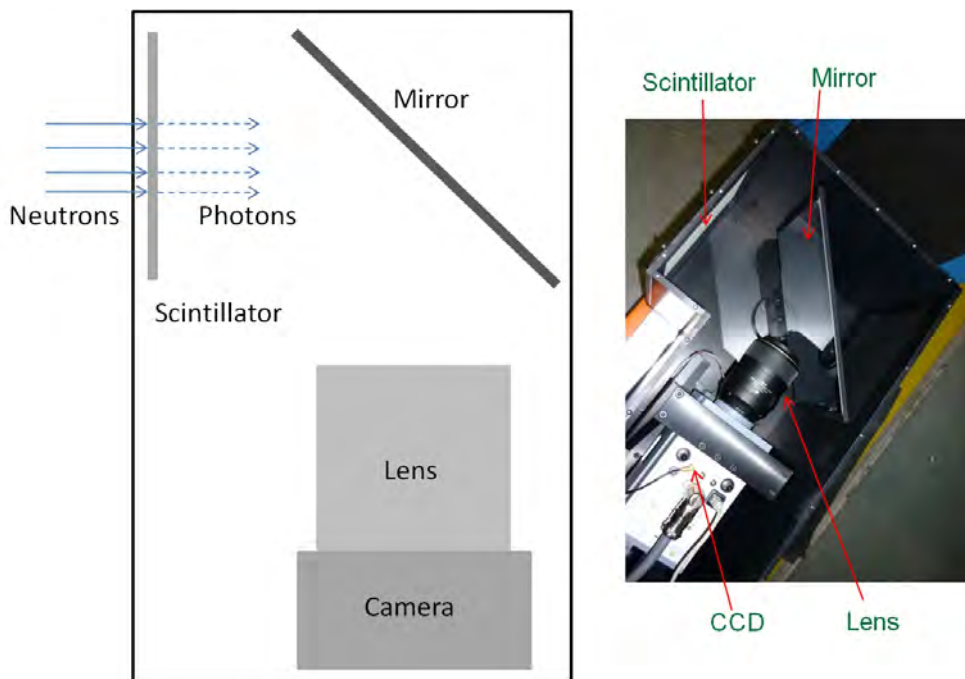

Fig. 6. Scintillator based neutron imaging device.

MCPs are thin slabs of material with an array of holes through the slab. Each hole or microchannel is an electron multiplier, so once a single electron is produced the signal is amplified by a 1000 times or more to enable detection of the single event. MCPs are glass based and have been developed for neutron imaging through the incorporation of ^{10}B in the glass. Interactions of the neutron with ^{10}B in the glass produces ions that can escape the glass into neighboring microchannels. These ions free electrons in the microchannel which then get multiplied and detected at the output. The latest microchannels are being produced with diameters <10µm leading to resolutions approaching 10µm. MCPs doped with ^{10}B are efficient for neutron detection due to the high cross section of ^{10}B. Efforts to improve these devices further are attempts to further reduce the channel diameters for higher resolution and doping with Gd to further improve efficiency (Tremsin, 2011).

3.1.3 System design

Due to the difference in available source spot sizes, radiography system geometries in particular used for CT differ between x-ray and neutron systems in the position of the object between the source and detector. Neutron systems place the object as close as possible to the detector while x-ray CT systems place the object half way between source and detector. One reason x-ray systems will place object in the center is to allow rotation of source and detector around the object for CT. This isn't possible with the permanent neutron sources, so the object must be rotated and doesn't need to be centered. Another advantage of placing the object in the center is a magnification factor of two for the object projection on to the detector. Magnification eases resolution requirements for the detector, but restricts size of the source spot to maintain resolution.

Resolution of radiography systems (both x-ray and neutron) is determined by source size, system geometry, and detector resolution. Detectors for both x-ray and neutron imaging systems consist of a conversion material, optics, and a pixelated detector. Resolution of the detector is a function of the point spread of the conversion material, the modulation transfer function of the optics, and the pixel size of the pixelated detector. Resolution of an imaging system up to the detector plane is a result of the source and system geometry as shown in figure 7. In this figure, an edge is imaged by a source of finite size, D, at a distance, L, from the source. From parts a and b of the figure, the blur of the edge which is called penumbra, p, is obviously smaller with the reduced source size. The comparison between a and c shows an inverse relationship between the source to detector distance and the penumbra. As a result, instrument developers at neutron sources often specify the quality of their neutron beams with L/D. This value has a direct relationship to resolution of the beam for imaging. L/D values from 300-500 are typical at neutron imaging instruments. Most instruments will offer setups at several different L/D values. The L/D values are selected by placing an aperture in the beam line close to the source to restrict the size of the source. As the diameter of the aperture gets smaller, L/D (resolution) increases linearly and exposure time increases as a square of the diameter. Since one could easily produce a very high L/D value with a small aperture an instrument specifications must also include a neutron flux value for fair comparison between imaging instruments.

The example in figure 7 kept the object at the same distance from the imager. To understand why the object is placed close to the imager for neutron imaging with a relatively large spot size, consider the effect of pulling the object away from the imager. If an object is placed in

contact with the imager, penumbra is reduced to zero. As the object moves away, the object is magnified onto the detector, but so is the penumbra or blur of the edges. For flexibility, neutron imaging instruments have stages to move the object position setup to accommodate various size objects and still keep them as close to the imager as possible.
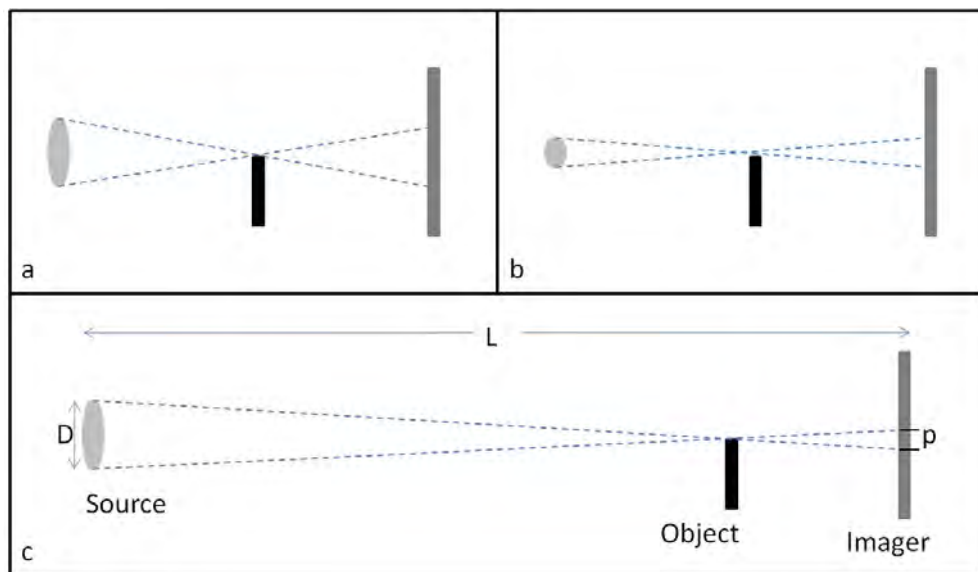

Fig. 7. Resolution of system depends on source size and geometry. Decrease in source size between a and b; Increase in source to detector distance between a and c.

Before a user submits a proposal to use a neutron imaging instrument, he/she should understand the capabilities of the beam line to determine whether the instrument provides the required field of view and resolution for their application. User facilities have specifications for their beam lines and will provide best resolution and field of view specifications, but it is difficult to include all potential imaging setups in descriptions of a neutron imaging instruments due to the flexibility. User facilities have beam line scientists assigned to each instrument. Consulting with the beam line scientist on a particular application is a recommended method to determine whether the instrument is capable of meeting the needs for the proposed research.

3.2 Data management

Data management at large-scale research facilities can be drastically different than commercially available smaller scale systems. In general commercially available system are static as well as propriety and perform in a highly regulated environment whereas research facilities are quite dynamic and utilize open source packages on unregulated open data files. Many research facilities do indeed have data policies and/or best practices that they follow but for the most part they follow an open research policy. These large-scale research facility

data policies support an innovative and collaborative environment while still enabling a fair and competitive atmosphere.

In recent years we have seen a dramatic increase in data file sizes that are generated from research instruments. This size increase has afforded researchers the ability to produce high fidelity images with extremely fine-grained resolutions. As a result, scientific discovery has been enabled and it is now commonplace to process and transfer data files on the order of hundreds of gigabytes. These data files are part of collections that in some cases approach a terabytes of raw and reduced data. The ability to transfer these data sets over high-bandwidth modern networks is now not trivial especially when remote users require these data collections to be transferred to their home institutions. In most cases it is necessary to use multi-threaded streaming data file transfer applications in order to efficiently migrate these data collections. For instance, Orbiter Commander is currently used at the Spallation Neutron Source for transferring data collections utilizing streaming compressed mutli-threaded algorithms as seen in figure 8.
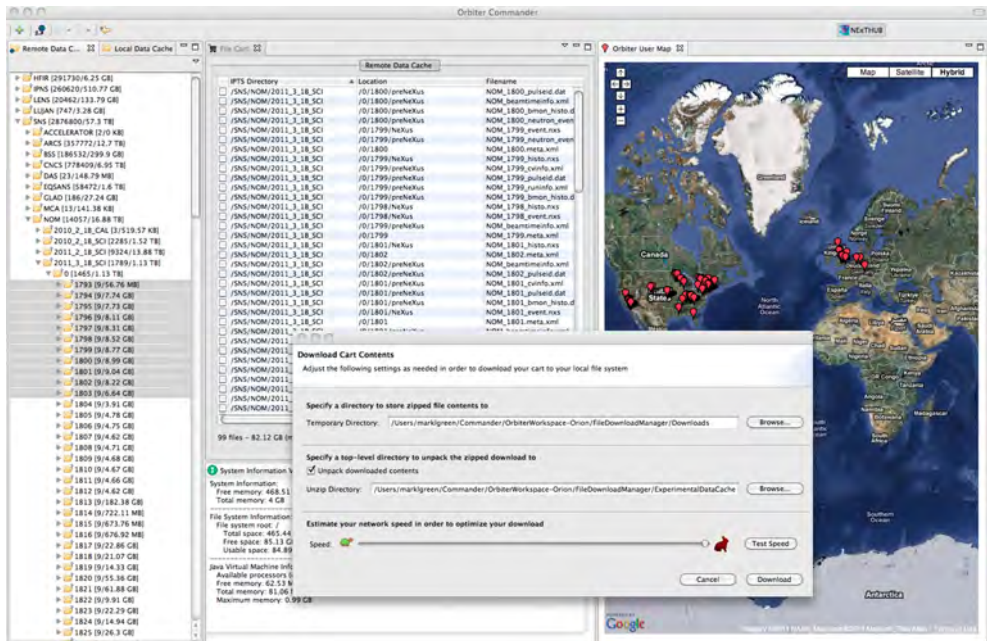

Fig. 8. The Commander file download manager application – https://orbiter.txcorp.com

3.3 Data reduction and normalization

Data from scintillation based detectors results in projections stored in common image storage formats. MCP imagers detect individual neutron interactions resulting in a list that includes the time and position of each acquired interaction instead of an image. Images are produced out of this list mode data through binning of the individual interactions based on the imaging setup (i.e. binning on time for pulsed sources provides energy resolution). X-ray CT systems encountered in medical imaging applications are well developed such that

projection data is captured along with normalization shots and then normalized and passed to a reconstruction engine without requiring input from the user along the way. The flexibility of neutron imaging instruments makes full automation of this process difficult, since the user can select the number of projections, range of angles, number of normalization images, and rotational stage position. Acquisition will provide the user with a projection data set and normalization images (light and dark) based on the setup. Beam lines will have normalization and reconstruction capabilities for the users to analyze their data.

After acquisition, the sample data files produced need to be normalized. The normalization is a simple mathematical process that cleans up the data by removing imperfection of the incident beam, signal detected that are not related to the sample measured and noise due to the surrounding. To perform the normalization, two more data files called open beam and dark field are required.

The open beam measures the shape and intensity of the incident beam. The open beam is acquired using exactly the same set up and time duration as the sample data file but without the sample in the beam. Due to the way they are acquired, background signals of the open beam and sample data have to match. Because the intensity of the incident beam can vary over time, it is important to bring the intensity of the data file background to the same level as the open beam background. This is done by selecting several regions of interest, away from the sample, in the data file, and calculating their average intensities. The same process is repeated on the open beam. Average of the ratio of those intensities gives a corrector factor to apply to the sample data. The dark field measured the electronic noise (thermal noise and dark current) and background. It is acquired with incident beam turn off and shutter open.

Gamma rays detected also need to be removed from the various files. Gamma rays events have the particularity of being very concentrated (1 or 2 pixels for each event) and very intense. Because those events happen randomly, the files have to be treated individually. Different mathematical processes can be used to do so. In development of normalization routines at ORNL, we discovered that the Lee filtering works very well. After removing gamma strike spikes from all images include data, open beam and dark field, the data are normalized using the following mathematical formula:

$$ND = \frac{Data - DF}{OB - DF}$$

With ND: normalized data, Data: data sample, DF: Dark Field and OB: Open beam. Since the DF and OB images are used to normalize every projection, any noise in these images propagates into all normalized projections. To reduce the noise in the normalization images, multiple DF and OB images are collected and averaged together after removal of gamma spikes.

To facilitate this whole process, programs such as iMars, (iMAging Reduction Software), as shown in figure 9, can be used. This program, using the IDL[24] programming language, has been developed at the Spallation Neutron Source and works as follows. First, the user has to select the input files (data file, open beam and dark field) and select the regions of interest

---

[24] IDL: http://www.ittvis.com

using manual or graphical input. The program then automatically performs the normalization and produced various output file formats (fits, tiff or jpeg).
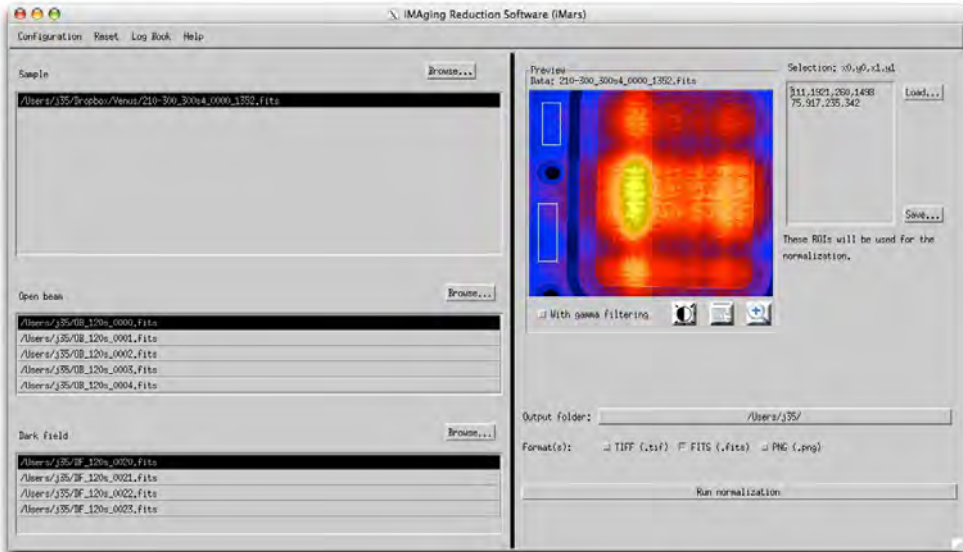

Fig. 9. iMars (iMAging Reduction Software) user interface in use with the HFIR imaging beamline.

3.4 Data reconstruction

Neutron radiography and computed tomography reconstruction can fully leverage techniques of medical imaging with x-rays and has benefited from the development of analysis and reconstruction algorithms developed by the medical imaging community. Two discrete classes of reconstruction algorithms are widely employed to generate tomographic images. Analytic algorithms calculate the image data directly using defined single-pass mathematical methods. These algorithms have the advantage of relative simplicity and speed, but tend to produce noisier reconstructed images. In contrast, iterative reconstruction algorithms employ complex models of the acquisition system and repeatedly estimate solutions and compare the estimate with a modeled "ideal" solution until pre-defined convergence criteria are met. Iterative algorithms typically produce superior images but can take much longer to execute. We will briefly introduce these two types in this chapter, and a more detailed treatment can be found in (Gleason et al., 2010).

As an example of an analytic type, Filtered Back Projection (FBP) algorithms are well developed for cone beam geometries seen in x-ray CT systems (Kak, 1988). Neutron radiography systems are cone beam systems as well and therefore use the exact same reconstruction algorithms with a change in system parameters for placement of the center of rotation closer to the detector. Again, flexibility of the neutron systems will challenge the user to set up the appropriate system parameters in any reconstruction code used so attention must be paid to the setup during data acquisition to ensure a proper reconstruction.

FBP basically spreads the attenuation measured by a single pixel within a projection equally across the 3D volume between the source and the pixel. With enough projections around the object, the attenuation on a true object piles up and the attenuation that is spread to incorrect positions in the volume becomes insignificant. This direct calculation method enables high speed reconstruction of 3D volumes, but places requirements on number and spacing of projections around the object. These requirements are easily met by x-ray systems due to the high flux from x-ray sources. Neutron sources have lower flux at the camera, so obtaining a data set with sufficient signal to noise ratio and number of projections may not be feasible due to time required to collect the projections.

Iterative reconstruction algorithms have seen considerable development for improvement of x-ray CT data, but do not see common use in medical imaging outside of research environments, because iterative reconstruction is computationally intense requiring much more time than FBP, and FBP reconstructions are suited for most medical applications. A CT projection data set represents a large set of linear equations to be solved for attenuation in each voxel of the volume. Using iterative methods for solving linear equations, reconstruction codes have been developed by many research groups with variation in the iterative methods focused on speeding up reconstruction through quicker convergence or parallel computation. Iterative reconstruction algorithms allow reconstruction with fewer and non-uniformly distributed projections and allow inclusion of more complex physics models. For these reasons, iterative algorithms should be considered as a reconstruction option for neutron radiography where the number and quality of projections are less than in medical x-ray CT. However, iterative reconstruction comes at a considerable cost in computation.

3.5 Image analysis and data visualization

In broad use across the national laboratories is a wide range of open-source and commercially licensed image analysis and data visualization applications. To illustrate, several are listed below:

IDL[25]**:** The Interactive Data Language (IDL) is a commercial array-processing language, which has been designed from its earliest inception for image processing applications development. IIDL implements an efficient array-processing engine combined with a large library of analysis routines, and is well suited for rapidly developing a wide variety of complex mathematical programs. This combination of array processing, image visualization, and data analysis functionality is why IDL is well suited for the tomography reconstruction. While a full version of IDL requires a license from ITT Visual Information Systems (ITTVIS), the IDL Virtual Machine is freely available and able to run compiled IDL programs. IDL is also capable of exporting compiled procedures as self-contained executables, making it an ideal platform for developing and sharing tomography algorithms.

MATLAB[26]**:** MATLAB is commercial a high-level array language with control flow statements, functions, data structures, file and data input/output, and object-oriented programming features with an integrated interactive development environment, and has pre-built extensive facilities for displaying vectors and matrices as graphs, as well as

---

[25] IDL: http://www.ittvis.com/
[26] MATLAB: http://www.mathworks.com/

capabilities for annotating and printing these graphs. It includes high-level functions for two-dimensional and three- dimensional data visualization and image processing. MATLAB is also a natural platform for rapidly prototyping and developing reconstruction algorithms.

VisIt[27]**:** Developed by Lawrence Livermore National Laboratory, VisIt is a free, open source, interactive parallel visualization and graphical analysis tool for viewing scientific data on Unix and PC platforms. Users can quickly generate visualizations from their data, animate them through time, manipulate them, and save the resulting images for presentations. VisIt contains a rich set of visualization features so that you can view your data in a variety of ways. It can be used to visualize scalar and vector fields defined on two- and three-dimensional (2D and 3D) structured and unstructured meshes. VisIt was designed to handle very large data set sizes in the terascale range and yet can also handle small data sets in the kilobyte range.

VisIt employs a distributed and parallel architecture in order to handle extremely large data sets interactively. VisIt's rendering and data processing capabilities are split into viewer and engine components that may be distributed across multiple machines:

VisIt-Viewer: Responsible for rendering and is typically run on a local desktop or visualization server so that it can leverage the extremely powerful graphics cards that have been developed in the last few years.

VisIt-Engine: Responsible for the bulk of the data processing and input/output (I/O) and is typically run on a remote compute server where the data is located. This eliminates the need move the data and makes high-end compute and I/O resources available to it. The engine can be run serially on a single processor or in parallel on thousands of processors.

VisIt also supports C++, Python and Java interfaces. The C++ and Java interfaces make it possible to provide alternate user interfaces for VisIt or allow existing C++ or Java applications to add visualization support. VisIt can be controlled by its Graphical User Interface (GUI), through the Python and Java programming languages, and can be integrated into custom user interfaces as well.

VTK[28]**/ITK**[29]**:** The VTK is an open source library, licensed under the GPL (section 1.1). It is entirely written in C++ and is available for many different platforms (Linux, Mac and Windows), and has support for writing platform independent applications. The library has a size of over 700 C++ classes and contains many algorithms for 2D and 3D image processing and visualization. It implements a data processing pipeline and numerous filters for reading, modifying and writing data. It also implements algorithms for volume and surface rendering. Although the library is written in C++, it was designed to be easily extensible and can be used within other programming languages. There are currently wrappers available for TCL/TK, Java and Python. For the surface rendering, VTK typically uses OpenGL to make use of the graphic card's hardware acceleration. In contrast to that, volume rendering will in most cases be performed "in software" by the computer's CPU.

---

[27] VisIt: https://wci.llnl.gov/codes/visit/

[28] VTK: http://www.vtk.org/

[29] ITK: http://www.itk.org/

ITK is an extension of the VTK, adding techniques for analyzing medical images, for example and registration/segmentation methods. Like the VTK, the ITK comes with an extensive class documentation that has the same features as the VTK documentation. ITK also includes several example applications that demonstrate the functionality of the library.

ImageJ[30]**:** ImageJ is a public domain Java image-processing program inspired by NIH Image for the Macintosh. It runs, either as an online applet or as a downloadable application, on any computer with a Java 1.4 or later virtual machine. Downloadable distributions are available for Windows, Mac OS, Mac OS X and Linux.

It can display, edit, analyze, process, save and print 8-bit, 16-bit and 32-bit images and read many image formats including TIFF, GIF, JPEG, BMP, DICOM, FITS and "raw". It supports "stacks", a series of images that share a single window. It is multithreaded, so time-consuming operations such as image file reading can be performed in parallel with other operations.

ImageJ does calculate area and pixel value statistics of user-defined selections and mea- sure distances and angles. It can create density histograms and line profile plots and it supports standard image processing functions such as contrast manipulation, sharpening, smoothing, edge detection and median filtering. It does geometric transformations such as scaling, rotation and flips. Image can be zoomed up to 32:1 and down to 1:32. All analysis and processing functions are available at any magnification factor. The program supports any number of windows (images) simultaneously, limited only by available memory. Spatial calibration is available to provide real world dimensional measurements in units such as millimeters. Density or gray scale calibration is also available.

ImageJ was designed with an open architecture that provides extensibility via Java plugins. Custom acquisition, analysis and processing plugins can be developed using ImageJ's built in editor and Java compiler. User-written plugins make it possible to solve almost any image processing or analysis problem.

GPULib[31]**:** Graphics hardware has been increasing in performance at a much faster rate than CPUs. Additionally, since they are designed for graphics applications, GPUs already include a great deal of parallelism and are optimized for vector- and matrix-based calculations. Until recently this power was used mostly for video games and computer-generated animations, and now the scientific community is taking advantage of GPU performance in visualization applications routinely. GPULib is a commercial product which provides a high-level, generalized interface that allows scientists and engineers to take advantage of the speed and performance of GPU hardware in their own applications. Using GPULib, vector calculations, matrix transforms, and array manipulations can be off-loaded from the CPU to NVIDIA graphics hardware, leveraging the optimizations and speed of the GPU to increase performance of their applications. Currently, language bindings for IDL, Matlab, Python, Java, and C exist. Generally GPULib can be integrated quickly and provide 30-100x speedup for reconstruction algorithms and 3D tomography visualizations.

---

[30] ImageJ: http://rsbweb.nih.gov/ij/
[31] GPULib: http://www.txcorp.com/products/GPULib/

GPULib can be used within all of these steps for increasing the processing speed substantially. To use GPULib from within an IDL script, you first need to call the gpuinit procedure. This will load the needed libraries and give you access to GPU-related functions. Once gpuinit is loaded, you will have access to over 135 GPULib functions.

4. Case study – Neutron imaging

Following is a case study examining the utility and issues for neutron based medical imaging. Currently there are no known neutron detection based commercial medical imaging scanners, though medical applications for neutron imaging are explored.

4.1 Medical applications of neutron imaging

Interest in neutron radiography dates back to shortly after Chadwick's discovery of the neutron (Chadwick 1932). In the 1950's and 1960's, neutron radiography came into use in non-destructive testing(Berger 1965) but it was the later when it interest in imaging biological samples emerged(Thewlis 1956; Berger and McGonnagle 1962; Barton 1964; Atkins 1965). Seminal articles on the subject outlined to problems of neutron detection, radiation dose, and multiple scattering events for in realistic thicknesses of tissue that degrade the images for everything but high energy neutrons (> 1 MeV)(Brown and Parks 1969; Parks and Brown 1969; Budinger, Bichsel et al. 1971; Budinger, Howerton et al. 1971). At that time, images were obtained by using a scintillator that exposed photographic film. Since that time, detectors have improved and cover much more of the energy spectrum than would be required to perform any imaging in humans. Despite advances, current detectors are specific for defined neutron energies, are not linear, and do not cover the entire energy spectrum (Vartsky, Mor et al. 2005; Marinelli, Milani et al. 2006; Marinelli, Milani et al. 2007; Mayer, Forkel-Wirth et al. 2007; Dangendorf, Bar et al. 2009; Mor, Vartsky et al. 2009; Ruddy, Flammang et al. 2009; Ruddy, Seidel et al. 2009; Vartsky, Mor et al. 2010).

The most significant problem for neutron imaging of tissues is multiple neutron scattering by the protons in hydrogen. The best transmission images, x-ray or neutron, occur when there is only a single scattering event in the sample before it reaches the detector. This goal is never practically achievable. A larger the percentage of multiple scattering events will result in greater the degradation of the image. Since tissue is composed of hydrocarbons, neutron radiography is currently confined to thin specimens or the neutron energies must be large. This is best understood by considering the scattering of neutrons from the protons in hydrogen atoms in the organic molecules that compose tissues.

From elementary kinematics, the energy transfer from the incident neutron to the proton (where the masses of the neutron and proton are taken to be equal) is given by:

$$E_p = \frac{1}{2}E_n\left(1 - \cos\phi\right)$$

where E_p is the recoil proton energy, E_n is the incident neutron energy, and ϕ is the center of mass scattering angle. Averaging over all scattering angles gives a result that on the average; the energy is divided evenly between the neutron and proton, i.e.

$$E_p = \frac{1}{2}E_n.$$

So even very energetic neutrons are converted to thermal neutrons (energy ~0.025 eV) within relatively few collisions. It can easily be shown that a 10 keV neutron requires ~19 collisions to reach a thermal energy while a 10 MeV neutron will only 28 collisions before becoming completely thermalized. After a very few collisions, the neutron distribution becomes isotropic and thus has lost all structural information. To understand how this applies to tissues, consider Table 1 which shows an approximate composition of human tissues (this will vary somewhat between organ systems but it is representative of the body as an average). The cross sections are for thermal neutrons only and $N\sigma$ represents the total elastic cross section as measured in the laboratory. This shows that the neutrons are scattered more by hydrogen than the next most significant element, carbon, by a factor of 20. Deuterium, which is hydrogen with a neutron or ^2_1H, has a much smaller cross section for neutrons and therefore will not attenuate the beam as much. Thus, by using deuterated or heavy water, the number of multiple scattering events will decrease which will improve the image. The total cross section is important because it is related to the mean free path by:

$$\lambda = \left(\sum_i N_i \sigma_i \right)^{-1}$$

where the i's refer to the different elements present. As noted above, most of the scattering is from the proton in hydrogen so the mean free path in tissues can be approximated by:

$$\lambda \approx \frac{1}{(N_H \sigma_H)}.$$

Element	Tissue Abundance	Atomic Weight	Number Density (cm^{-3})	σ (b)	$N\sigma$(cm^{-1})
H	0.11	1.008	6.51E+22	30.39	1.977084
C	0.51	12.010	2.53E+22	4.746	0.120158
N	0.02	14.010	8.51E+20	12.19	0.010372
O	0.36	16.000	1.34E+22	3.97	0.053320
Na	0.001	22.990	2.59E+19	3.92	0.000102
P	0.001	30.970	1.92E+19	4.37	0.000084
S	0.001	32.070	1.86E+19	1.52	0.000028
Cl	0.001	35.450	1.68E+19	65.32	0.001099

Table 1. A representative elemental composition of human tissues with number densities, thermal neutron ($E_{thermal}$ = 0.025 eV) cross sections, and total elastic scattering cross sections.

Table 2 shows the mean free path for neutron energies from 1 eV to 10 MeV for hydrogen scattering only. The table shows that to penetrate a human limb that the incident neutron spectrum will need to be between 1 and 10 MeV. As might be expected, increasing the neutron energy also increases the radiation dose (absorbed dose). The exact details of such radiation doses due to a neutron require a significant effort to calculate. Such calculations are typically performed by large Monte Carlo codes such as available from the Radiation Safety Information Computational Center at Oak Ridge National Laboratory[32]. Prior determinations of neutron doses would indicate that doses would be in an acceptable range but further work needs to be performed before human trials could be contemplated (Brown and Parks 1969; Budinger, Howerton et al. 1971; Kry, Howell et al. 2009).

E(keV)	σ(b)	Nσ(cm-1)	λ(cm)
0.001	20.470	1.33256	0.750
0.01	20.181	1.31380	0.761
0.1	20.153	1.31196	0.762
1	20.048	1.30510	0.766
10	19.196	1.24867	0.800
100	12.743	0.82957	1.205
1,000	4.246	0.27643	3.617
10,000	0.935	0.06088	16.427

Table 2. Neutron cross sections, total neutron cross sections, and mean free path lengths for hydrogen, as a function of energy.

One method to ameliorate the attenuation problem is to change the water composition from normal water to deuterated water (also referred to as heavy water)(Slatkin, Stoner et al. 1983; Nakagawa, Hatanaka et al. 1994; Kushner, Baker et al. 1999; Medina, Li et al. 2005). Studies have shown that approximately 20% of total body water (TBW) can be replaced with deuterated water without deleterious effects(Kushner, Baker et al. 1999). However, it is time consuming to replace 20% of the TBW, which would require several days of intravenous or oral deuterated water intake. Since deuterated water is also expensive, this is not currently a likely method to improve neutron transmission through tissue *in vivo*.

Even though there are problems with neutron attenuation and tissue dose for neutron imaging, there are real possibilities for the future. Images have been made of small amounts of tissue as can be seen in Figure 10. The images are of a rat lung in two views. The trachea, main stem bronchi and bronchial tree are well defined by the contrast afforded by air bronchograms. Several orders of bifurcation are clearly seen. Additionally, the cartilaginous rings in the trachea and main bronchi are clearly visible as well showing a difference in

---

[32] RSICC at ORNL: http://rsicc.ornl.gov

contrast between the two types of connective tissue. The cartilaginous bands are separated and covered by a fibrous connective tissue. The molecular composition and thickness is seen in the images. As detectors improve and imaging system geometries improve the resolution of such images will undoubtedly improve. Resolutions of 50-10 µm are readily available at most neutron imaging centers today. Resolutions of 1 µm appear to be routinely possible in the near future with sub-micron imaging a real possibility in the future.
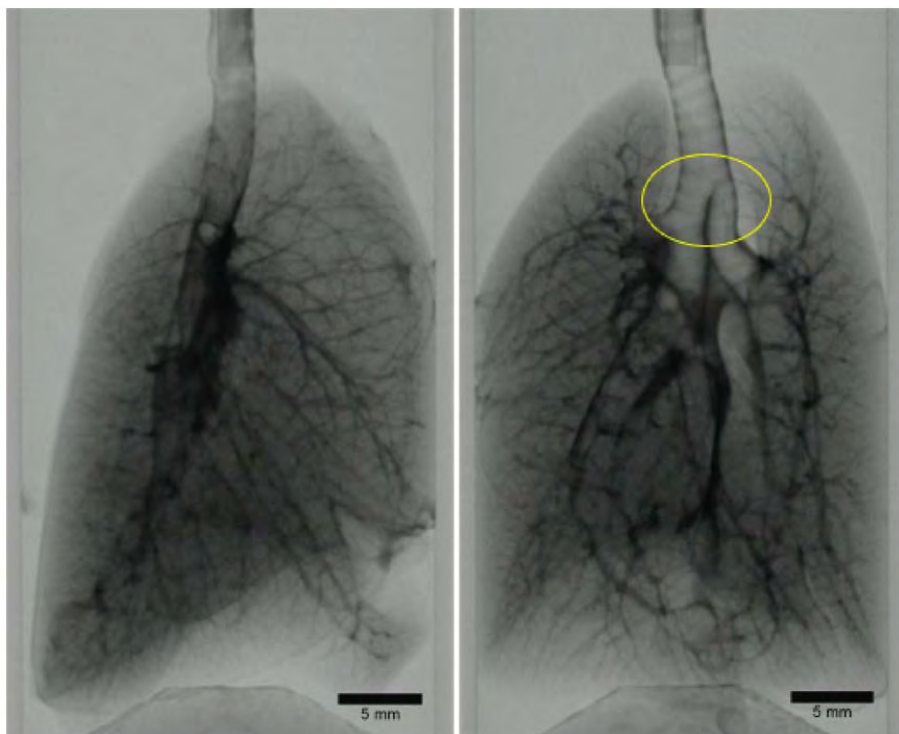
Fig. 10. Two neutron radiographs of the lungs of a rat from lateral (left) and anterolateral (right) views are shown. The air bronchograms are clearly visible as is the cartilaginous rings in the trachea and main bronchi. Courtesy: Dr. Burkhard Schillinger, Neutronentomographie ANTARES, Forschungsreaktor FRM-II, Technische Universität München, Germany.

4.2 Possible uses

Osteoarthritis (OA) is the most common of all joint diseases affecting 68% of persons over 68 years of age as based upon radiological criteria(Goldman and Ausiello 2008). Clinically, patients suffer from pain and functional limitations such as decreased range of motion and instability. Plain x-ray radiographs demonstrate osteophytes and joint space narrowing. Currently, there exist no treatment strategies that prevent or ameliorate the disease process so therapies are aimed at analgesia and improving the function of the joint. Not infrequently, the patient has a chronic course that eventually fails medical therapy which

makes the patient a candidate for joint replacement surgery. When the joint has significant functional limitations and/or the pain becomes intractable, interfering with sleep or activity the patient may elect to have a total joint replacement. The bone prosthesis interface is very important to the success of the procedure. Even though not common, total knee replacement infection rates are 0.5 to 1.0 whereas total hip replacements have infection rates of 0.5 to 1.0 (1995; Berbari, Hanssen et al. 1998; Sperling, Kozak et al. 2001; Widmer 2001). It is important to make an accurate diagnosis because the treatment is the removal of the prosthesis followed by many weeks therapy with antibiotics. New prostheses are not always possible after infection. Therefore, it is very important to be certain that there an area of infection next to the metal. X-ray techniques such as CT suffer from significant degradation due to scattering from the metal prosthetic device. MRI scanning can still produce suitable images except in the case of cardiac pacemakers and defibrillators. The prevalence of cardiac pacemakers in all Medicare beneficiaries was increasing in time with 504.4 per 100,000 enrollees in 2000 as compared to 324.5 in 1990 and the prevalence increases significantly with age (Brown, Croft et al. 2005). So the patients with pacemakers or defibrillators and joint prostheses are increasing which leads to diagnostic dilemmas when the prosthesis is believed to be infected. Using a technique called Bragg edge imaging, the bone prosthesis interface should be amenable to relatively high resolution imaging which should demonstrate the fluid found in an infection in those patients with pacemakers.

Another case which is becoming far too common is that of a stroke patient who needs an MRI of the brain but cannot due to a pacemaker. Since both MRI and neutron radiography map the hydrogen atom distribution to create an image, neutron radiography should be able to provide images that would allow an accurate diagnosis to be made. Whether this is actually achievable will require more research.

Like positron emission tomography, magnetic resonance imaging, and x-ray computed tomography before it, neutron radiography will much research and engineering for it to become a clinically useful tool. Paul Lauterbur and Raymond Damadian doubtless had people shake their heads when told that their machines would image water in the body when that is the major constituent of the human body. They eventually developed the MRI which has revolutionized medical imaging of certain structures such as the brain. Originally, the MRI could not image the heart, lungs, or great vessels due to motion and slow acquisition rates. Those problems with time are being solved. So there is good reason to believe that neutron imaging could have a similar story. Since the mean free path of a positron is ~1 mm, it has been felt that PET cannot exceed a resolution of 1 mm. However, improved reconstruction algorithms are improving the resolution to the sub-millimeter range. Thus, it is reasonable to believe that the barriers for using neutron radiography for *in vivo* human imaging will be overcome. When that occurs, physicians will have new images that will improve their understanding of some disease processes and aid in the care of their patients.

5. Conclusion

The national laboratories provide a number of imaging and scattering instruments which can be used to facilitate basic medical research. These resources are available competitively via the scientific peer review process for proposals submitted through the user programs operated by each facility. Imaging human and animal tissue occurs but is not routine in most places, and strict procedures must be followed to do so. However research

communities are burgeoning in a number of biomedical areas, and protein crystallography research is well established in the X-ray and neutron scattering communities. Novel here is the forward looking work on neutron imaging with potential medical and biomedical applications. Thus the national laboratories provide a research environment with capabilities and a culture conducive to researching new methods and techniques suitable for exploring new frontiers in medical and biomedical imaging.

6. Acknowledgement

7. References

Arai, M. & Crawford, K. (2009). Neutron Sources and Facilities, In: *Neutron Imaging and Applications*, H. Z. Bilheux, R. L. McGreevy, & , I. S. Anderson, pp. 13-30. Springer, ISBN 978-1-4419-4619-5, New York.

Atkins, H. L. (1965). "Biological evaluation of neutron radiography." Materials Evaluation 23: 453-458.

Baker, G. A.; Heller, W. T. (April 2009), Small-angle neutron scattering studies of model protein denaturation in aqueous solutions of the ionic liquid 1-butyl-3-methylimidazolium chloride, *Chemical Engineering Journal*, Vol. 147, No. 1, pp. 6-12, Available from:
http://www.sciencedirect.com/science/article/pii/S1385894708007250

---

[33] BES Operations: http://science.energy.gov/~/media/budget/pdf/sc-budget-request-to-congress/fy-2012/Cong_Budget_2012_BES.pdf

Barth H. D., Launey, M. E. MacDowell, A. A. Ager III, J. W. Ritche, R. O. (2010), Irradiation Effects on Human Cortical Bone Fracture Behavior, *ALS Science Highlight #212.*

Barton, J. P. (1964). "Some Possibilities of Neutron Radiography." Physics in Medicine and Biology 278: 33-42.

Beckmann, E.C. (2006). CT scanning the early days, *The British Journal of Radiology*, Vol 79. (January 2006) pp 5-8, DOI: 10.1259/bjr/29444122

Berbari, E. F., A. D. Hanssen, et al. (1998). "Risk factors for prosthetic joint infection: case-control study." Clin Infect Dis 27(5): 1247-54.

Berger, H. (1965). Neutron Radiography. New York, Elsevier Press, Inc.

Berger, H. and W. J. McGonnagle (1962). Progress on neutron radiography, Argonne National Laboratory. USAEC Report ANL-6279.

Brown, D. W., J. B. Croft, et al. (2005). "Epidemiology of pacemaker procedures among Medicare enrollees in 1990, 1995, and 2000." Am J Cardiol 95(3): 409-11.

Brown, M. and P. B. Parks (1969). "Neutron radiography in biologic media. Techniques, observations, and implications." The American journal of roentgenology, radium therapy, and nuclear medicine 106(3): 472-85.

Budinger, T. F., H. Bichsel, et al. (1971). "Visual phenomena noted by human subjects on exposure to neutrons of energies less than 25 million electron volts." Science 172(985): 868-70.

Budinger, T. F., R. J. Howerton, et al. (1971). "Neutron radiography and dosimetry in human bengs: theoretical studies." Physics in Medicine and Biology 16(3): 439-50.

Chadwick, J. (1932). "Possible Existence of a Neutron." Nature 129(3252): 312.

Choi, H. J. & Weis, W. I. (2011), Crystal Structure of a Ridig Four-Spectrin-Repeat Fragment of the Human Desmoplakin Plakin Domain, *Mol. Biol.*, Vol 409, No. 800, DOI: 10.1016/j.jmb.2011.04.046.

Dangendorf, V., D. Bar, et al. (2009). "Multi-Frame Energy-Selective Imaging System for Fast-Neutron Radiography." Ieee Transactions on Nuclear Science 56(3): 1135-1140.

D de Jonge, M.; Vogt, S. (2010). Hard X-ra fluorescence tomography – an emerging tool for structural visualization. *Structural Biology*, Vol. 20, No. 5, pp. 606-614. DOI : 10.1016/j.sbi.2010.09.002.

Giri, N. C.; Sun, H., Chen, M., Costa, M., and Maroney, M. J., (2011), XAS Structural Investigation of Early Intermediates in the Mechanism of DNA Repair by Human ABH2, *Biochemistry*, DOI: 10.1021/bi101668x

Gleason, S.; Paulis, M., & Osborne, D. (2010). Molecular Imaging: Principles and Practice: Principles of Micro X-ray Computed Tomography, Weissleder, R., et al., eds., McGraw Hill, 2010, ISBN 9781607950059

Goldman, L. and D. Ausiello, Eds. (2008). Cecil Medicine. Philadelphia, Saunders, Elsevier.

Gupta, A. & Kielkopf, C. L. (2011). Purification, Crystallization and Preliminary X-ray Crystallographic Analysis of a Central Domain of Human Splicing Factor 1, *Acta Crystallogr.*, F 67, No. 486. DOI: 10.1107/S1744309111004623.

Hinerman, J. M. (2008). The Study of Protein-Protein Interactions Involved in Lagging Strand DNA Replication and Repair, Dissertation – University of Toledo, Available from:http://etd.ohiolink.edu/send-pdf.cgi/Hinerman%20Jennifer%20M.pdf? toledo1216824884

Jorgensen, S.; Eaker, D. Vercnocke, & A. Ritmin, E. (2008). Reproducibility of Global and Local Reconstruction of Three-Dimensional Micro-Computed Tomography of Iliac Crest Biopsies, *IEEE Transactions in Medical Imaging*, Vol. 27, No. 4, pp. 569-575.

Kak, A.C. and Slaney, M. (1988), *Principles of Computerized Tomographic Imaging,* IEEE Press.

Kushner, D. J., A. Baker, et al. (1999). "Pharmacological uses and perspectives of heavy water and deuterated compounds." Can J Physiol Pharmacol 77(2): 79-88.

Litzlbauer, H.; Korbel, K. Kline, T. Jorgensen, S. Eaker, D. Bohle, R. Riterman, E. & Langheinrich, A. (2010). Synchrotron-Based Micro-CT Imaging of the Human Lung Acinus, *Anatomical Record*, Vol. 293, No. 9. pp 1607-1614.

Marinelli, M., E. Milani, et al. (2006). "High performance (LiF)-Li-6-diamond thermal neutron detectors." Applied Physics Letters 89(14).

Marinelli, M., E. Milani, et al. (2007). "Synthetic single crystal diamond as a fission reactor neutron flux monitor." Applied Physics Letters 90(18).

Mayer, S., D. Forkel-Wirth, et al. (2007). "Response of neutron detectors to high-energy mixed radiation fields." Radiation protection dosimetry 125(1-4): 289-92.

Medina, D. C., X. Li, et al. (2005). "Pharmaco-thermodynamics of deuterium-induced oedema in living rat brain via 1H2O MRI: implications for boron neutron capture therapy of malignant brain tumours." Phys Med Biol 50(9): 2127-39.

Mor, I., D. Vartsky, et al. (2009). "High spatial resolution fast-neutron imaging detectors for Pulsed Fast-Neutron Transmission Spectroscopy." Journal of Instrumentation 4.

Moritz, R.; Eaker, D. Langheinric, A. Jorgensen, S. Bohle, R. & Ritman, (2010), E. Quantification of Vasa Vasorum Density in Multi-Slice Computed Tomographic Coronary Angiograms : Role of Computed Tomographic Image Voxel Size, Journal of Computer Assisted Tomography, Vol. 34, No. 2, pp 273-278.

Nakagawa, Y., H. Hatanaka, et al. (1994). "Partial deuteration and blood-brain barrier (BBB) permeability." Acta Neurochir Suppl (Wien) 60: 410-2.

Nelson J.; Huang, X. Steinbrener, J. Shapiro, D. Kirz, J. Marchesini, S. Neiman, A. M. Turner, J.J. Jacobson, C. (2010), High Resolution x-ray diffraction microscopy of specially labeled yeast cells, PNAS, Vol. 107, No. 16, DOI: 10.1073/pnas.0910874107.

Parks, P. B. and M. Brown (1969). "Antiscatter grids for low-energy neutron radiography." Radiology 92(1): 178-9.

Pynn, R. (1990). Neutron scattering A PRIMER, *Los Alamos Science*, Vol. 19, http://library.lanl.gov/cgi-bin/getfile?19-01.pdf

Rao, D.; Cesareo, R. Brunetti, A. Akatsuka, T. Yuasa, T. Takeda, T. Tromba, G. & Gigante, G. (2009). Micro-CT Imaging of Rat Bone and Lumber Vretebra using Synchrotron Radiation, *Application of Accelerators in Research and Industry : Twentieth International Conference*, Vol. 109, pp 896-899.

Ruddy, F. H., R. W. Flammang, et al. (2009). "Low-background detection of fission neutrons produced by pulsed neutron interrogation." Nuclear Instruments & Methods in Physics Research Section a-Accelerators Spectrometers Detectors and Associated Equipment 598(2): 518-525.

Ruddy, F. H., J. G. Seidel, et al. (2009). "Development of Radiation Detectors Based on Semi-Insulating Silicon Carbide." 2008 Ieee Nuclear Science Symposium and Medical Imaging Conference (2008 Nss/Mic), Vols 1-9: 5256-5262.

Slatkin, D. N., R. D. Stoner, et al. (1983). "Whole-body irradiation of deuterated mice by the 10B(n, alpha)7Li reaction." Proc Natl Acad Sci U S A 80(11): 3480-4.

Sperling, J. W., T. K. Kozak, et al. (2001). "Infection after shoulder arthroplasty." Clin Orthop Relat Res(382): 206-16.

Stock, S.; De Carlo, F. & Almer, J. (2008). High energy X-Ray scattering tomography applied to bone. Journal of Structural Biology, Vol. 161, No. 2, pp. 144-150. DOI: 10.1016/j.jsb.2007.10.001.

Stoltz E.; Yeniguen, M. Kreisel, M. Kampschulte, M. Doenges, S. Sedding, D. Ritman, E. Gerriets, T. & Langhinrich, (2011). Angioarchitectural Changes in Subacute Cerebral Venous Thrombosis, *NeuroImage*, Vol. 55, pp. 1881-1886.

Thewlis, J. (1956). "Neutron radiography." British Journal of Applied Physics 7: 345-350.

Tremsin, A.S., Phate, J.B., Vallerga, J.V., Siegmund, O.H.W., Feller, W.B., Lehmann, E., and Dawson, M.(2011), "Improved efficiency of high resolution thermal and cold neutron imaging," Nuclear Instruments and Methods in Physics Research Section A: Accelerators, Spectrometers, Detectors, and Associated Equipment, Vol. 628, No. 1, pp. 415-418.]

Uchida, M.; McDermott, G. Wetzler, M. Le Gros, M. A. Mylls, M. Knoechel, C. Baron, A. E. & Larabell, C. A., (2009), Soft x-ray tomography of phenotypic switching and the cellular response to antifungal peptoids in Candida albicans, Proc. Nat. Acad. Sci., Vol. 106, No. 46.

Vartsky, D., I. Mor, et al. (2010). "Novel detectors for fast-neutron resonance radiography." Nuclear Instruments & Methods in Physics Research Section a-Accelerators Spectrometers Detectors and Associated Equipment 623(1): 603-605.

Vartsky, D., I. Mor, et al. (2005). "Time-resolved fast neutron imaging: simulation of detector performance." Nuclear Instruments & Methods in Physics Research Section a-Accelerators Spectrometers Detectors and Associated Equipment 542(1-3): 206-212.

Widmer, A. F. (2001). "New developments in diagnosis and treatment of infection in orthopedic implants." Clin Infect Dis 33 Suppl 2: S94-106.

Xiao, X.; Xia, D. Bian, J. Han, X. Sidky, E.Y. De Carlo, F. & Pan, X. (2010). Image reconstruction from sparse data in synchrotron-based micro-tomography of biomedical samples, 1st International Conference on Image Formation in X-Ray Computed Tomography, UCAIR, pp 156-164.

Xiao, X.; De Carlo, F. & Stock, S. (2008). X-ray zoom-in tomography of calcified tissue, *Developments in X-Ray Tomography SPIE proceedings*, Vol. 7078. DOI: 10.1117/12.796638.

Zhang, Y.; Lagi, M., Liu, D. Z., Mallamace, F., Frantini, E., Baglioni, P., Mamontov, E., Hagen, M., Chen, S. H. (2009), Observation of high-temperature dynamic crossover in protein hydration water and its relation to reversible denaturation of lysozyme, *Journal of Chemical Physics*, Vol. 130, No. 13, Available from:
http://jcp.aip.org/resource/1/jcpsa6/v130/i13/p135101_s1